Post-Print

When citing this work, cite the original published paper.

Permanent link to this version
http://hdl.handle.net/11311/1063012

Development of an Intrusive Technique for Particles Collection in Rockets Plume.

Stefania Carlotti[a,*], Filippo Maggi[a], Alessandro Ferreri[a], Luciano Galfetti[a], Riccardo Bisin[a], Dominik Saile[b], Ali Gühlan[b], Christopher Groll[c], Tobias Langener[c]

[a]*Politecnico di Milano, Via La Masa 34, 20156 Milano, Italy*
stefania.carlotti@polimi.it · filippo.maggi@polimi.it · alessandro.ferreri@mail.polimi.it · luciano.galfetti@polimi.it · riccardo.bisin@polimi.it

[b]*German Aerospace Center DLR, Supersonic and Hypersonic Technology Department, Linder Höhe, 51147 Cologne, Germany*
dominik.saile@dlr.de · ali.guhlan@dlr.de

[c]*European Space Agency (ESA/ESTEC), Keplerlaan 1, 2201 AZ Noordwijk, Netherlands*
christopher.groll@esa.int · tobias.langener@esa.int

Abstract

An intrusive technique for particles capturing in supersonic-high temperature flows for the use in solid rocket motors plume characterization is proposed. A supersonic probe for the collection of the condensed combustion products in the proximity of the rocket nozzle has been sized to handle a progressive deceleration and cool down of the exhaust gas, preventing from liquid particles breakup. A quasy-1D gas dynamics software (POLIRocket-V2) based on the Shapiro method and normal shock wave theory, supported by a CFD investigation using the DLR TAU code, was employed for the feasibility and the design study. Preliminary cold flow tests have been performed in the supersonic vertical wind tunnel at DLR in relevent environment as a proof of concept of the probe working principle and the collection methodology studied.

Keywords: Supersonic flow, Solid rocket motors plume, Condensed Combustion Products, Shapiro, Cold Flow Tests.

---

[*]Corresponding author

Nomenclature

English symbols

A	Area
c	Speed of sound
C_p	Specific heat at constant pressure
C_v	Specific heat at constant volume
D	Hydraulic diameter
f	Fanning friction factor
k	specific heat ratio
L	Length
L^*	Mixing length
M	Mach number
M_m	Molar mass
MR	Mass ratio
$\dot{m}$	Mass flow rate
P	Static pressure
P_t	Total pressure
Q	Heat
R	Universal gas constant
R_{gas}	Gas constant
Re	Reynolds Number
s	Entropy
T	Temperature
V	Velocity
W	Work
x	Distance along the probe axis
X_{vap}	Fraction of evaporated mass
y	Radial distance from the axis
y^+	Dimensionless wqall spacing

Greek symbols

ϵ	Nozzle area ratio
ρ	Density

Acronyms

CCP	Combustion Condensed Product
CFD	Computational fluid dynamics
EMAP	Experimental Modelling of Alumina Particulate in Solid Booster
ODE	Ordinary differential equatio
TRP	Technology Research Program

Subscripts and superscripts

cool	Cooling flow
e	Properties at nozzle exit
g	Cooling gas
in	Inlet
mix	Ref. to mixing duct
out	Outlet
quench	Quenching fluid
stat	Static flow peoperties
tip	Ref. to the tip
tot	Total flow peoperties
vap	Evaporated flow
wall	Ref. to a wall

1. Introduction

The addition of aluminum powder to solid propellants allows an increase of the gravimetric specific impulse. However, the incomplete combustion of aluminum leads to the formation of condensed (solid or liquid) combustion products, which are detrimental in terms of performances and pollution. Reydellet [1] estimated that about 10% of the ideal specific impulse is lost in solid rocket motors and, out of this amount, about 1/3 to 2/3 is due to two phase losses. In fact, during nozzle expansion, the thermal and kinetic inertia of the large condensed particles lead to a warmer and slower flow with respect to the ideal gas-only case [2]. Additionally, latest studies have shown that alumina particles contribute among others to radiation from the plume [3] and may have a significant ozone depletion effect [4], due to the condensation of chlorine and moisture on solid particulate suspended in the atmosphere [5][6], suggesting the need to further study the reactivity and lifetime of alumina.

In the past decades great effort was put for the collection of combustion products in the vicinity of the burning surface and in the combustion chamber [7]-[11]. However, since both kinetic and thermal inertia are functions of the particle size, which changes significantly through the nozzle [12]-[15], the morphology of the agglomerates at the burning surface is not sufficient to fully understand their overall effects on motor performance and environmental pollution. Hence, CCPs collection during rocket tests at nozzle exit section is essential.

It is quite obvious that the high temperature and velocity of the plume makes the experimental activity extremely difficult. Authors main ideas consisted in the use of impinging surfaces well behind the rocket exhaust [8][16][17]. This kind of collection assumes that the morphology of the impinging particles is not altered by the impact with the capturing surface and the sample, though limited, is a representation of the total particle population. However, Gossé et al. [8] and Brown and McArty [17] pointed out that the possible effect of shock waves and particle growth in the exhaust plume, leading respectively to liquid particle shattering and coalescence, were not taken into account. Moreover, according to Kessel et al. [18], placing the collecting system well behind the rocket nozzle may be ineffective since the exhaust particles may have de-

parted the exhaust stream before capture. In this respect, reactions with air needs to be avoided. As suggested by literature [4][19], alumina particles would be convered by water accelerating the production of HNO_3 on their surface: this mechanism seems to be responsible for global ozone losses. In other cases, operators tried to collect as much material as possible by enclosing the rocket in collection systems or by operating suction devices with particle extraction features [20][21]. The tank collection method gave a measure of the detailed size distribution averaged over the duration of firing [20], highlighting that the particle size distribution is pressure-dependent when aluminized propellants are used. Some patents [22] with the scope to remove solid pollutants from rocket plumes were produced in the past. Such systems handled the full plume of the rocket and performed a particle-gas separation by using liquid quenching and filtering. Even though a good representation of the particle statistics is achieved, the size of the apparatus is large and not conceived to maintain the properties of the collected material. Kessel [18] studied several devices (subsonic and supersonic) having the capability of particle capturing by means of suction or ingestion. The capability of supersonic ingestion was always considered an added benefit since the absence of a bow shock at the front of the probe could avoid particle deviation and alteration. As a drawback of such configurations, these devices collect particles after filters.

In this scenario, ESA initiated the activity called Experimental Modelling of Alumina Particulate in Solid Boosters (EMAP), an international cooperative action leaded by DLR-Cologne (Germany) and involving FOI (Sweden) and SPLab-Politecnico di Milano (Italy). A subscale solid rocket motor, whose exhaust features shall resemble the properties of Ariane 6 plume, is going to be fired in a supersonic wind tunnel to simulate the flight status of the launcher at an altitude between 13 and 22 km. The objective of the activity is to assess relevant parameters about SRM plume features in small scale experiments and to develop and qualify measurement equipment for plume characterization. The dataset can be used for the validation of numerical simulations, which then in turn may be transferred to large scale SRMs. The parameters in detail concern the mean size, span, distribution, particle morphology, chemical composition, and temperature of Al_2O_3 particulate outside of the nozzle as well as aspects of the jet fluid itself like temperature, velocity, pressure and species concentration. In this

4

scenario, a novel intrusive technique has been developed to enable the CCPs collection in proximity of the nozzle exit section and their post analysis, in order to characterize the particle size distribution. The conceived sampling device targets the ingestion of the largest CCPs, trapped in the center of the expanding flow, mainly responsible for performance losses. On the contrary, since the smallest alumina particles will likely deviate from the axial direction and will settle in the lateral part of the expanding flow, they will be the target of other non intrusive optical techniques developed and improved in the EMAP scenario.

The present paper proposes the development of an intrusive technique for the CCPs collection conceived in the ongoing EMAP project. The paper is organized as follows. The first section describe the conceptual and detailed design, focusing on the requirements and the main aspects of the collection device. Then, the POLIRocket-V2 software developed to adequately support the design choices is presented, together with the CFD simulation verification campaign performed by ESA using the DLR TAU solver. The comparison between the results in some peculiar operating cases gave the sensitivity of the reliability limits regarding the simplified Shapiro approach implemented in the POLIRocket-V2 code in such a complex scenario. Finally, off-design cold flow tests are presented. The main aim of the experimental activity was the preliminary assessment of both the conceptual design of the probe and of the collection methodology proposed.

Table 1: SPLab particles collection device: main requirements and features.

Requirements	Features
Trap particles inside the plume	Supersonic inlet flow cooled and slowed down
Operational time: 0.5 s	Passive thermal management
Fast reconditioning	Liquid quenching for particles collection
Particle post collection analysis	

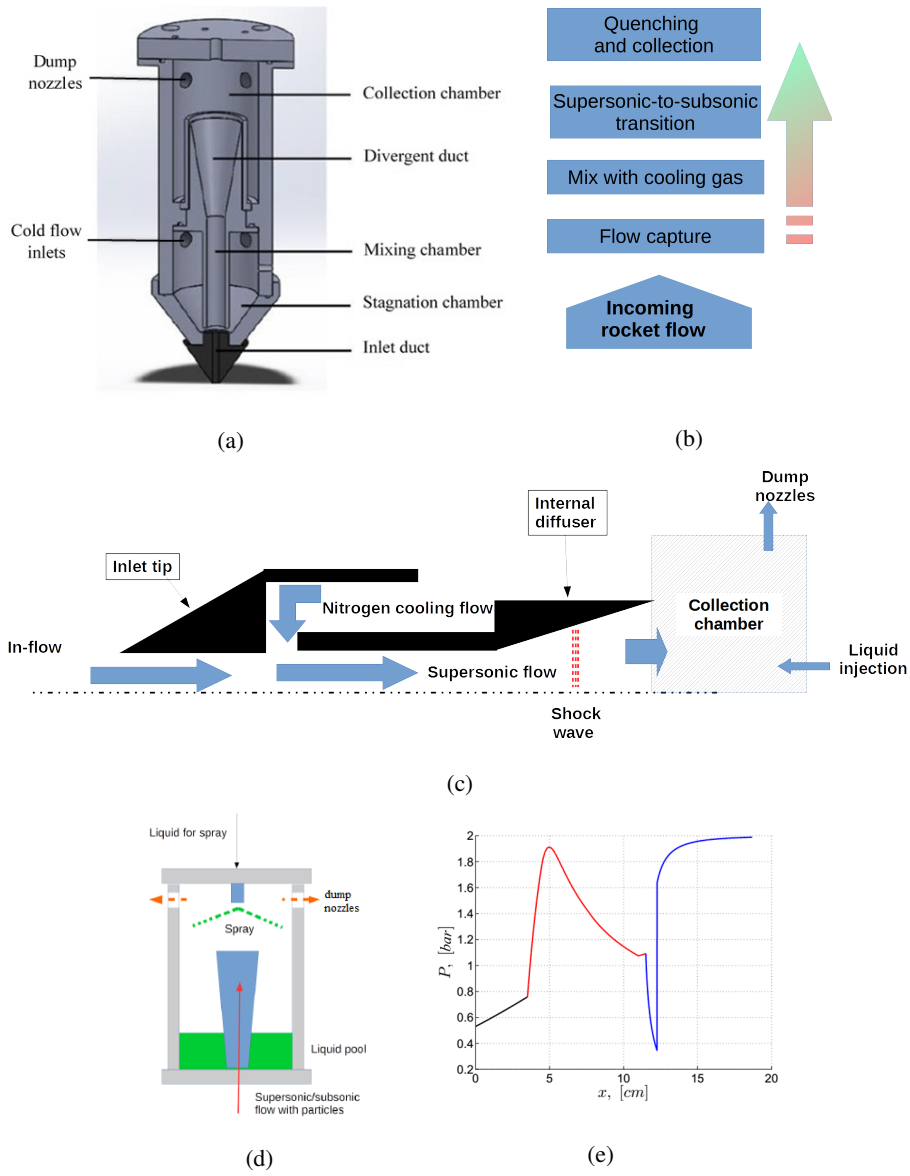5

(a)

(b)

(c)

(d)

(e)

Figure 1: SPLab supersonic probe: (a) construction scheme; (b) logical work flow; (c) internal scheme of probe design concept (d) Schematic functioning of the injector; (e) static pressure.

2. Conceptual and Detailed Design

The SPLab supersonic probe has been sized merging the technique of Kessel [18] and Carns [22]. The former swallows a supersonic hot flow and cools it down by the mixing with a cold inert gas; the latter captures the condensed particles by means of a quenching liquid spray. The schematic mechanical drawing and the flow chart of the conceived design are shown in Fig. 1. For the sake of clarity during the design description, the static pressure trend is also reported (Fig. 1e). Main requirements and features of the device are briefly summarized in Table 1, while detailed design analysis follows. The probe will supply a representative data set of the largest CCPs in the rocket plume and will be located in proximity of the nozzle exit section. Theoretical exhaust conditions are listed in Table 2. Since the supersonic medium in which the CCPs are suspended is likely to generate a bow shock in front of any object placed in the wake, the first component - the tip in Fig. 1a- has been shaped according to the supersonic flow past a cone theory [23]. The correct functioning of the collection device is strictly linked to the size and length of the tip. The inlet duct diameter has been sized to ingest a mass flow rate of approximately 0.0044 kg/s, granting a sufficient amount of CCPs entering the probe without the need to excessively increase the cooling mass flow rate. The tip length has been defined considering two main concerns: firstly, the deceleration of the flow in the inlet duct makes the temperature increase in excess of the melting temperature of alumina; secondly, the turbulent boundary layer growth together with a shock-train system may reduce the effective cross-section area up to a point where the flow becomes choked and a bow shock wave develops in front of the probe tip. This "unstart" of the probe will no further allow the collection of alumina particle.

Inside the device, the supersonic flow is subjected to a progressive deceleration and cooling in such a way that any strong shock is delayed, avoiding excessive temperature jump and particles break up. The flow will be subjected to a supersonic mixing with a cold inert gas in a straight channel (i.e., the mixing chamber in Fig. 1a) and to a supersonic-to-subsonic transition by means of a shock wave located in a divergent duct. In fact, the simultaneous decrease of the Mach number and temperature of the

7

Table 2: Theoretical exhaust condition. Propellant wt.% is AP 68%, Al 18%, HTPB 14%. (CEA code by NASA).

Mach number M, [-]	3.23
Static temperature T_{in}, [K]	2227
Static pressure P, [bar]	0.53
Molecular mass M_m, [g/mol]	26.3
Gas constant R_{gas}, [J/kgK]	317
Specific heat at constant pressure C_p, [J/kgK]	1888

flow only by varying the cross-section area of the duct or by means of a cooling jacket is impractical, since while temperature decreases the Mach number increases and the subsequent shock wave causes a strong temperature jump. According to Kessel [18], the mixing between exhaust gases and cold inert gas involves complex phenomena, such as boundary layer growth and formation of oblique shock waves. In particular, the choking of the flow caused by merging of different boundary layers or stagnant presence of the cooling inert gas inside the mixing chamber would lead to possible fluid dynamic instabilities. The former can be controlled if the channel has a divergent shape while the latter can be prevented by injecting the dilution gas at high speed. Hence, the mass flow ratio between the ingested flow and the coolant flow, the initial velocity and temperature of the latter have to be critically chosen. The coolant gas enters a stagnation chamber and reach the sonic condition in correspondence of the area entering the mixing chamber. Hence, a brief expansion assures a supersonic flow when encountering the ingested one. Radial injection in the mixing chamber was selected as the solution to achieve the best mixing (see Fig. 1).

The decelarating and cooling technique employed may give rise to concerns about eventual reactions of secondary gas with the particulates. Nitrogen was chosen as coolant since it is an inert gas. Typically it reacts with aluminum at high temperatures to form aluminum nitride. However, several propellant combustion devices and studies available in literature feature inert atmosphere of nitrogen [24][25][11] or use it to quench particles. Its effect was investigated and compared to the behavior of the same

propellants burning in different inert atmosphere, such as argon and helium. Negligible effects were highlighted on the burning rate and mean size of the CCPs [24][26]. Glotov et al. [27] identified a minor effect, enhanced with pressure, on the size distribution for aluminum particles with original size of 1.2-10 μm. However, since SRM plumes contain alumina particulate, no reactions with already oxidized aluminum is deemed to occurr.

Exiting the divergent, a scrubber acts in the collection chamber where particles are segregated from the gas using a quenching liquid sprinkler and are stored for post analysis. The collection chamber pressure is controlled in such a way that the supersonic to subsonic transition is generated as close as possible to the head-end of the divergent duct to avoid acceleration of the flow. Hence, it has to be comprised between the minimum and maximum possible pressure. The former is obtained by expanding the supersonic flow through the divergent duct and then placing a shock wave at the end of it (i.e., it is equal to the value of the pressure after the shock wave); the latter generates the shock wave at the probe inlet (i.e., it is equal to the value of pressure at the end of the duct). The desired pressure is set throughout chocked dump nozzles, granting a constant exiting mass flow rate.

On top of the quenching chamber a hollow-cone spray ensures the mist capturing the particles. A deflected spray was selected since it guarantees better stability for varying pressure over a limited interval in the chamber and it represents a better compromise between droplet size (about 100 microns), impinging velocity, and operating pressure. A spray angle of 120° was selected since it grants a wide spray cone and impinges on the internal wall of the collection chamber below the dump nozzles. A schematic representation of the injector functioning can be found in Figure 1d. Proper mass flow rate is discharged by the injector depending on the pressure differential between the collection chamber and the quenching liquid tank, pressurized by compressed air. Tetrachloroethylene has been selected as quenching liquid because its viscosity favors atomization and it evaporates without dissociating, hence avoiding undesired reactions with the combustion products. It must also be noted the consolidated experience gained by the SPLab team in terms of this kind of treatment of the CCPs detached by the

9

Table 3: Relevant Probe dimensions.

	Length L, [cm]	Diameter D, [cm]
Inlet Duct	3.5	0.5
Mixingh Chamber	8.0	1.3
Divergent Duct	7.2	3.7

burning surface and quenched. Quenching procedure and post analysis will immediately follow. The quenching procedure is confidential and it will not be detailed in the present work.

Since this measurement technique has been specifically developed for the small scale experimental activity that will be conducted at the Vertical Test Section Cologne (VMK), the sampling probe is assembled vertically, with the flow coming from the bottom. Minor revisions in the design of components will enable the use of the probe to full scale motor tests, usually conducted horizontally. Relevant dimensions are listed in Table 3. In order to grant the applicability of the probe to actual firing tests, a passive thermal management has been investigated in details:

- High machinable graphite has been selected for the tip component, granting its survivability at a stagnation temperature of about 3400 K and the manufacturing of straight edges;

- high temperature thermal protections have been successfully tested for the protection of the tip holder component and the pipings supplying both nitrogen and the quenching liquid.

Moreover, a movable refractory- and non-toxic based protecting shield will be placed between the exhaust and the probe, enabling the probe exposure to the flow for 1 s and protecting it throughout the rest of the test. Details on the experimental setup will be given in Section 5.1.

10

3. Fluid Dynamic Characterization: the POLIRocket-V2 code and the TAU Code

3.1. The POLIRocket-V2 code

The POLIRocket-V2 code, derived from a first implementation specialized in solid rocket motor internal ballistics [28], is a software based on a set of quasi-1D, steady-state, compressible gas dynamic equations where continuity, momentum, and energy are conserved. The form of the equations used in this solver have been developed by Asher H. Shapiro [23], who presented a method to deal with complex fluid dynamic problems having a strong one-dimensional transport nature. Different phenomena are taken into account: area variation, wall friction, heat exchange, mixing of gases which are injected into the main stream, as well as changes in molecular weight and specific heat. For details, the reader is encouraged to consult the original book by Shapiro [23]. The resulting equation set consists of 8 ODE relations, in logarithmic differential form, and 14 variables, six of them being independent. The system can be rearranged to obtain a space-marching solution. The main drawbacks of this approach are a critical sensitivity to $M = 1$ causing numerical instability and an underlying continuity requirement for variables. The solution is based on trapezoidal rule second-order accuracy method, integrating an initial-value problem [29]. The code is run from the tip to the shock and from the shock to the collection chamber. A constant discretization step is adopted, after proper grid-dependance sensitivity analysis. The code was numerically verified against different literature cases such as supersonic flow in presence of friction (Fanno flow model), heat addition (Rayleigh flow model), area variation (isentropic expansion), and global mass and enthalpy balance.

The code can be used in both on-design and off-design analysis. In the former case, the pressure in the collection chamber is set as design specification, deriving the rest of the probe properties (e.g. the exit area of the dump nozzles). In the latter case, geometric and inlet properties are fixed and the solver derives the new equilibrium pressure in the collection chamber.

3.2. The TAU Code

The numerical calculations presented here have been performed with the hybrid structured/unstructured DLR-Navier-Stokes CFD solver TAU [30]. A second order finite-

11

volume flow solver is applied to the RANS equations while the application of the AUS-MDV flux splitting scheme, in tandem with MUSCL gradient reconstruction, enables second order spatial accuracy. Turbulence modelling is implemented by means of the Spalart-Allmaras one-equation eddy viscosity model. The gas in the calculations presented here is considered as non-reacting, ideal gas.

3.3. Test Case

Table 4: Main features for POLIRocket-V2 code simulation.

| Component	Main Features
Inlet Duct	Adiabatic flow
	No enthalpy variation
	Friction: $f = \frac{0.0791}{Re^{0.25}}$ for $2.1 \times 10^3 < Re < 10^5$ [31]. Nominal expcted Re = 17×10^3
	Constant cross sectional area
Mixing Chamber	Supersonic mixing channel
	Adiabatic, non-isentropic flow due to friction
	Heat exchange: total enthalpy of the two gases (total temperature) per unit length variation
	to define the total enthalpy (total temperature) of the third gas, i.e. the mixture of the two
	Mass ratio MR and mixing length $L^\star$ assumptions
	Nitrogen: sonic condition in correspondence of the area entering the mixing chamber
	Progressive secondary flow addition (uniform differential mass flow rate addition)
	Local recomputation of average properties of the fluid (specific heats, average molar mass)
Divergent Duct	Shock wave theory [32]
	Constant area variation and friction effect
	Main input: collection chamber pressure
	Total enthalpy conservation
	Normal shock wave theory for computation of properties across the shock wave
Collection chamber	Stagnation conditions and choked dump nozzles
	Steady-state mass balance and enthalpy balance for pressure definition
	Evaporated mass fraction of C_2Cl_4 X_{ev} assumption
	Mass balance: final temperature computation

12

3.3.1. Domain and Boundary Conditions for POLIRocket-V2 code

The computation domain and boundary conditions (BCs) are based on the probe operational scheme reported in Figure 1. The initial BCs coincide with the themo-physical properties exiting from the upstream rocket nozzle, under the assumption of no front bow shocks (nominal inlet data listed in Table 2). The boundary conditions and the main features for each component are given in Table 4. The most important parameters affecting the flow behavior inside the probe are the following:

- Mass ratio: the ratio between the nitrogen and the ingested mass flow rate. Since it dictates the supersonic-to-subsonic transition, it defines if the sonic conditions are reached inside the mixing chamber;

- Mixing length: the assumed length in which the mixing between coolant and hot gases swallowed by the probe takes place, after which the flow is well stirred;

- Collection chamber pressure, dictating the shock wave location;

- evaporated mass fraction X_{ev}: the arbitrary assumed fraction of evaporated quenching liquid.

### 3.3.2. Domain and Boundary Conditions for TAU CFD Code

The computational domain used in the TAU calculations is derived from the cross section of the probe. Figure 2a shows the axisymmetric grid, which is generated for the probe geometry using the CENTAUR 11.5 hybrid grid generation package and subsequently refined by TAU's gradient-based mesh adaptation module. The grid consists of approximately 220000 nodes and employs prismatic layers to resolve boundary layers on viscous walls. These structured layers are adapted over the course of several computations, in order to ensure a dimensionless wall spacing of y^+=1 (see Fig. 2c). An adaptation process is also applied to the unstructured grid regions to increase the grid resolution at locations with substantial temperature, pressure and Mach number gradients with a mixed criterion. A detailed view of the grid within the inlet channel where the refined mesh reflects the complex flow at this location is given in Fig. 2b. This 2D mesh is extruded to a 1 degree wide wedge bound by Euler walls, as no swirl is considered in this computation.

13
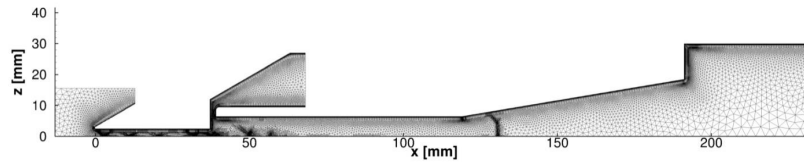
(a)
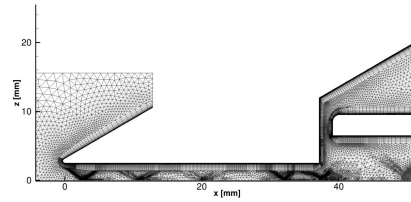
(b)
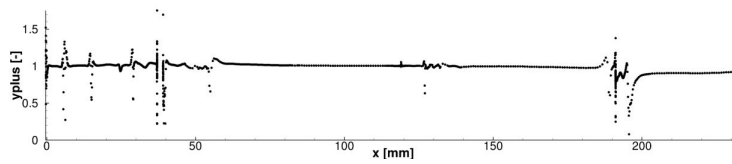
(c)

Figure 2: Axisymmetric domain for the TAU calculations: (a) Adapted mesh reflecting the velocity, pressure and temperature gradients encountered in the flow field (2 *bar* backpressure); (b) Detailed view of the adapted Mesh within the probe inlet and mixing duct (2 *bar* backpressure); (c) Plot of sampled y^+ values along the internal probe walls.

Upstream from the probe inlet, a far field boundary condition is employed to set up the flow encountered by the probe. The rotational geometry used in the computation presented here prohibits the inclusion of the discrete coolant injection points found in the real probe design. Therefore, only part of the coolant inlet plenum is modeled while the coolant input is realized by means of a reservoir-pressure inflow boundary condition on which the total pressure and total density of the coolant are fixed. The included inlet geometry then allows for the capturing of the effects caused by the redirection of the flow to the radial injection point. This represents a compromise between the low computational effort of quasi 2D calculations, which is desirable as a large number of coolant inlet and discharge pressure combinations are examined, and the inclusion
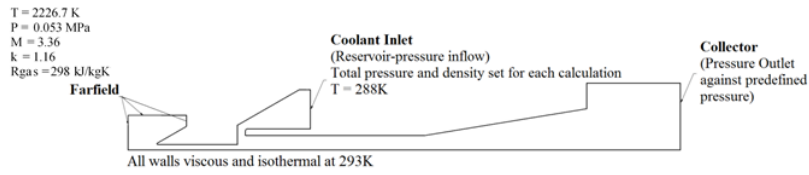
14

Figure 3: Overview of selected boundary conditions. The farfield is defined according to the values given in Table 2.

Table 5: Probe nominal parameters.

$L^*, [cm]$	$MR, [-]$	$P, [bar]$	X_{ev}
7.5	10.02	2	0.5

of flow effects caused by the complex internal geometry of the probe. The collection chamber is simplified as a cylinder whose discrete outlets of the probe are neglected and the expulsion of gas is facilitated via a constant pressure outlet boundary condition. With this configuration it is possible to predefine the collector pressure, which in the probe hardware is set up via calibrated orifices. An overview of the described setup is given in Fig. 3.

4. Results

4.1. Numerical Results

4.1.1. POLIRocket-V2 Code Results

The evolution of flow properties in the probe is highlighted in Figs. 1e and 4. Main probe parameters are listed in Table 5. The horizontal axis represents the coordinate inside the probe channel starting from the lip of the inlet tip. Three colors are identified in the figures, one per each part of the apparatus. The black curve represents the inlet duct. The inlet of the nitrogen cooling flow is placed at the end of this portion. The red curve corresponds to the mixing channel and the blue leg is representative of the internal divergent. The right-side end of the curve is the inlet condition for the quenching area, with the imposed collection chamber pressure.
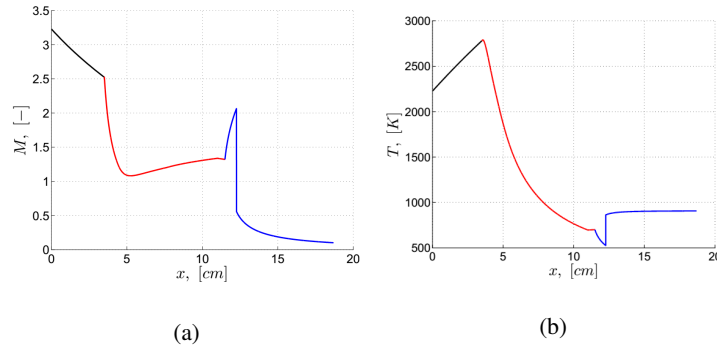
15

Figure 4: Flow properties computed with the (POLIRocket-V2 code: (a) Local Mach number; (b) Local static temperature.

- in the first part a straight channel with friction is present. This is a Fanno flow and a decrement of the supersonic Mach number is expected. In this section the total temperature is preserved while the total pressure decreases. A general increment of the static properties is visible since a decrease of the local Mach number is recorded. A temperature elevation greater than 2300 K is shown, causing alumina melting. However, considering the assumption of adiabatic channel and thus of a flow not transferring heat to the walls, it is reasonable to assume that the temperatures will be lower than the alumina melting one. In fact, in the reality, a heat removal occurs due to the thermal inertia of the tip material, which is at room temperature at the beginning of the test. Moreover, since the inlet boundary conditions are assumed to coincide with the themophysical properties exiting from the upstream rocket nozzle, the heat exchange between the plume and the external ambient, which would lead to an incoming colder flow, is not taken into account. In the light of above, solid particles are expected when the primary flow is mixed with nitrogen. However, the exact definition of the probe behavior requires an advanced strongly coupled multiphysics simulation, which is beyond the scope of the present work;

- in the second portion, the mixing is modeled as a progressive mass addition with corresponding increment of the main flow area. That is, in this portion the total properties vary locally, as the mixing process is distributed. Initially, the Mach

16

number strongly decreases because of the momentum balance. Then, the mass injection and the temperature reduction (and thereby the reduction of the speed of sound) lead to a further slight increase. The static pressure can be interpreted in a similar manner while the static temperature progressively decreases because of the cooling effect of the injected flow, and consequent reduction of the mixture total temperature;

- the divergent portion shows the typical behavior of an over-expanded nozzle modeled in a quasi-1D framework. A shock is located after an initial expansion and consequent acceleration. The Mach number sharply decreases, after an initial increment. The reported static properties increase.
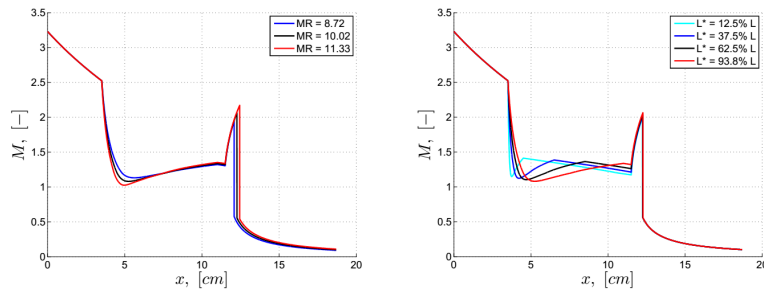
(a) Mass Ratio ($L^\star = 7.5cm$, $\dot{m}_{in} = 0.0044$ kg/s)

(b) Mixing Length ($MR = 10.02$, $\dot{m}_{in} = 0.0044 \, kg/s$)

Figure 5: Parametric studies on mixing process; the plots are representing the Mach number.

A parametric analysis has been conducted to identify the nominal condition of the probe, focusing on the four main parameters identified in Sec. 3.3.1. The conclusions of this set of computer runs are listed in Table 5 and briefly summarized as follows:

- the progressive increment of the coolant injection decreases the minimum Mach number obtained in the mixing duct and the location of the shock is shifted downstream. The nominal value is arbitrarily chosen to avoid chocking of the flow and a shock wave too close to the initial section of the divergent duct (see Fig. 5a);

- the mixing length does not strongly affect the global behavior of the probe. The longer the $L^\star$, the smoother the variation of the thermodynamic and fluid prop-

17

erties. The end of the mixing process coincides with a local maximum of the Mach number. The minimum value of the Mach in the mixing channel and the location of the shock are quite insensitive to this parameter. See (see Fig. 5b);

- greater values of the collection chamber are preferred, since they yields weaker shock waves and low Mach number at the end of the divergent. Moreover, the assumption of sonic dump nozzle requires high pressure in the collection chamber with respect to the environmental pressure. Hence, the pressure is set accordingly and the dump nozzles area derived;

- half of the C_2Cl_4 is supposed to evaporate or decompose once injected in the collection chamber. The real amount of X_{ev} can be estimated only after hot flow tests. However, the optimal dump nozzle diameter (and hence, in turn, the pressure inside the collection chamber and the shock wave location) is quite insensitive if different X_{ev} values are considered.

4.1.2. TAU Code Results

Computations have been performed for a wide range of coolant inlet and collector pressure combinations, while the far field conditions remain constant throughout the results presented here. Relevant cases are discussed in the following. The goal is the identification of an operational point with a different tool than the POLIRocket-V2 Code.

The probe's internal pressure needs to be set to a value that allows the flow into the probe to start, avoiding the generation of a bow shock. A detailed view of the results obtained for a computation where the collector pressure outlet boundary condition is set to 7 *bar*, while the total pressure at the coolant inlet boundary condition is also set to 7 *bar* in order to avoid flow out of the coolant inlet, is shown in Fig. 6a. It can be seen that hot gases do not enter the probe and that a bow shock is formed in front of the inlet because of cold gas escaping the probe through the inlet.

Reducing the pressure prescribed at the outlet boundary condition to 6 *bar* results in the establishment of the flow field indicated in Fig. 6b . The inclination of the shock corresponds to the nominal behavior of a cone exposed to a supersonic flow [32]. As in

18

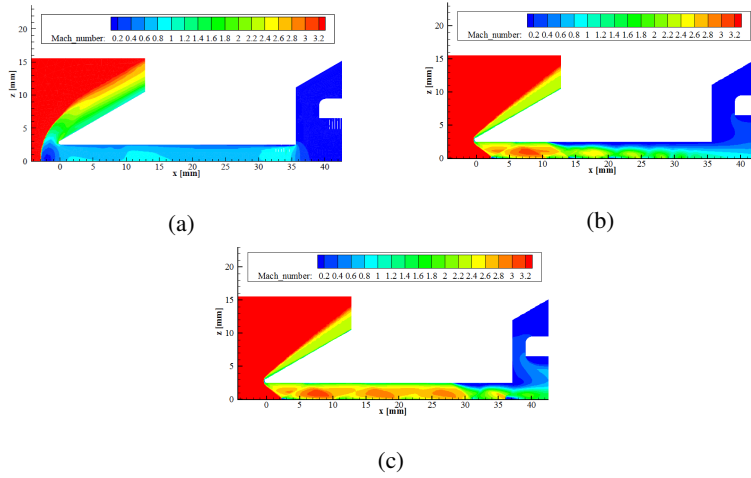(a)   (b)

(c)

Figure 6: Detailed view of the probe inlet: (a) a backpressure in excess of 7 *bar* prohibits the ingestion of hot gas and creates a bow shock in front of the probe inlet; (b) backpressure of 6 bar; (c) backpressure of 4 bar.

several aeronautical internal-diffusion supersonic intakes, an oblique shock train is generated inside the inlet duct [33]. However, the flow is still supersonic and progressively slows down through a set of weak shocks. Towards the end of the duct a boundary layer separation can be identified on the flow region close to the walls but such event does not propagate upwards and does not choke the inlet channel. While the probe now ingests hot gases from the external flow, the transition to subsonic speeds takes place before the flow has the opportunity to mix with the radially injected coolant.

Further reducing the backpressure to 4 *bar* while setting the coolant inlet condition to $P_{tot,coolant} = 4$ *bar* and $\rho_{tot,coolnat}$=4.66kg/m^3 mitigates this issue. A detailed view of the shock train present in the inlet channel is given in Fig. 6c while 7a gives an overview of the results for the entire domain. While the flow topology up to 1 *cm* downstream of the inlet remains identical to the 6 bar backpressure case, the flow remains sonic up to 7 *cm* downstream of the inlet. The transition to subsonic conditions is promoted by the addition of the coolant, which reduces the static temperature of the mixture flowing through the mixing chamber. An indication of the temperature of the ingested gas as it mixes with the radially injected coolant is given in Fig. 7b. The reader should be
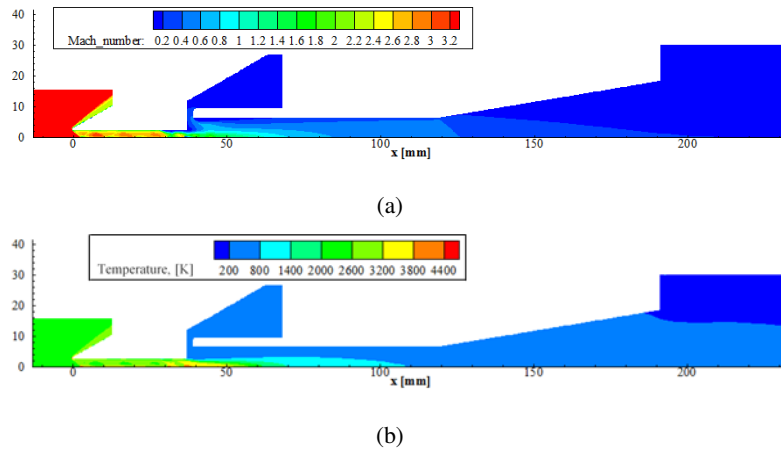
19

Figure 7: Flow field at 4 *bar* backpressure: (a) Mach number; (b) static temperature.

aware that adiabatic walls are considered in the simulation. The temperature in the core flow falls below the melting point of Alumina at approximately 7 *cm* downstream of the probe inlet. This gives the particles time to cool before they enter the collection chamber and interact with the fluid droplets that are being injected there. Also note that the width of the coolant inlet is reduced in the 4 *bar* backpressure case in order to arrive at the intended coolant mass flow rates.

The backpressure is now further reduced to 2 *bar*, while leaving the coolant inlet condition unchanged, in an attempt to obtain a supersonic-to-subsonic transition in the divergent duct.

The detailed view of the flow field in the inlet duct is shown in 8a. It can be seen that it is quite similar to that encountered in the 4 *bar* backpressure case. This is due to the radial injection of coolant just behind the inlet. The coolant impinges on itself, creating a zone of increased pressure, which limits the influence of downstream pressure variations on the inlet duct flow field. It can also be seen that the velocity within the radial cooling gas inlet increases due to the decreased pressure in the mixing duct. The overview plot of the Mach number in Fig. 8b also shows that the bulk of the fluid passing the mixing duct stays supersonic and even accelerates when it reaches the divergent section of the duct. The acceleration of the gas is accepted here as this pressure combination allows the particles to cool and solidify in a high velocity flow
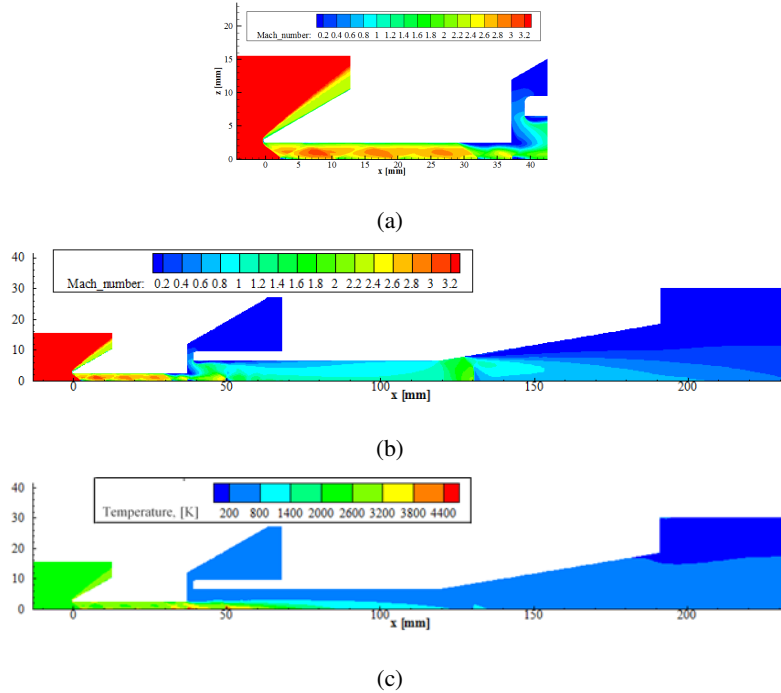
20

(a)

(b)

(c)

Figure 8: Backpressure of 2 *bar*: (a) Flow field within the probe inlet; (b) Mach number; (c) Static temperature.

before being subject to high velocity gradients. Figure 8c gives an insight into the temperature distribution within the flow. It can be seen that the length of the mixing channel is sufficient for the hot gas to mix with the injected cold gas before entering the collector.

4.1.3. Comparison and Discussion

The simulation results discussed above are now compared to the results generated by the POLIRocket-V2 code. With respect to the Shapiro code, the CFD analysis ensures higher degree of details including turbulence modeling, oblique shock determination, and boundary layer development. On the other hand, the Shapiro code represents an appealing engineering approach due to its straightforwardness and low computational demands. Hence, these two approaches are complementary and a comparison between them is essential to assess the quality of the Shapiro code.

21

Static pressure, static temperature and Mach number data are extracted from TAU computations. Data sampling points are located on the rotational axis at one millimeter intervals throughout the internal probe flow path up to the end of the divergent duct. Due to the large variation of these variables over the radius of the flow passages, data averaged over the channel cross section are also extracted at identical axial positions. For the extraction of the static pressure the area averaging technique is used while temperature and Mach number averages are generated using a mass flow weighted averaging approach.

The POLIRocket-V2 software was modified to include the inlet rounding effect as modelled in the mesh of the TAU code. In both cases the same Mach number of M=3.36, the same gas properties of k=1.16 as well as R_{gas}=298 J/kgK were adopted. The other thermodynamic properties were modified accordingly. This new condition enabled the same inlet mass flow rate through the tip. The POLIRocket-V2 code could not implement the nominal coolant-to-inlet mass ratio of 10.9 due to sonic point instability. The value was set to 10.4 for this code only.

The numerical CFD simulations reported in this paper were carried out including the effect of the round on the leading edge of the probe tip as per specification of the manufacturing tolerances. This round effectively increased the diameter available for gas to enter the probe by roughly 0.6 mm and, in turn, affecting the ingested mass flow rate slightly. On the other hand, the POLIRocket-V2 code considered a straight inlet duct, neglecting the construction roundness.

The comparison of meaningful results is performed by showing both punctual data on the probe axis and the section-averaged values along the channel:

- as shown in Figure 9, the TAU code identifies a strong fluctuation along the inlet duct for Mach number, static temperature, and static pressure. This is caused by the oblique shock train in the inlet duct, visible also in Figure 6c. The POLIMI-V2 code cannot detect this event and presents a smooth behavior. When the TAU averaged properties are considered, the resulting Mach number in the inlet duct is lower than the one provided by the Shapiro approach. As a consequence,
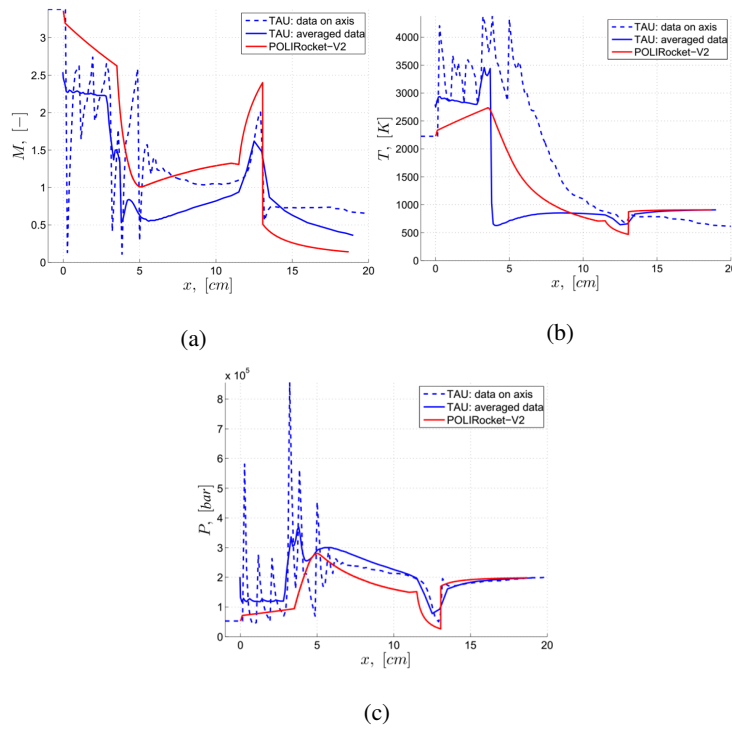
22

Figure 9: 2D axial-symmetric vs. quasi 1D comparison: Mach number: (a) Mach number, (b) Static temperature; (c) Static pressure.

the temperatures and the pressures are higher. The trend can be justified by the difference in the inlet section. The presence of a rounded inlet in the 2D domain creates a short convergent channel which causes a reduction of the Mach number with respect to the ideally straight inlet modeled by the POLIMI-V2 code;

- once the main flow reaches the mixing chamber, a sudden Mach number decrement is observed by the POLIMI-V2 code because of the mixing with the cooling flow. The same process is visible in the CFD approach but data is clearer when the curves with the averaged properties are considered. The injected coolant flow impinges on the main flow creating a subsonic region for the length of the mixing duct. The trend observed by the Shapiro approach is the same but also in this case an overestimation is obtained.

23

- for the divergent portion, both the codes approximately agree on the definition of the shock wave location. The CFD analysis reveals the presence of oblique shocks in the divergent portion and the shock is not planar. Such details cannot be detected by the quasi-1D approach where this supersonic-to-subsonic transition is observed as a discontinuity.

Globally, the Shapiro approach features the same trend as the CFD results in terms of averaged quantities. However, some discrepancies are present. The flow presents a strong bi-dimensional property due to shock generation. The boundary layer is minimally influencing the flow. Another interesting point is represented by the effect of the coolant injection. According to the standard CFD approach, a subsonic region is present at the injection of the nitrogen, whereas the POLIRocket-V2 observes the proximity of a sonic condition but the flow is not reaching it. In any case, the trend matching is very good and the capability of capturing the shock wave location is valuable.

5. Experimental Activity

The experimental activity aims at being a proof of concept of probe functioning in off-design conditions represented by a cold flow tests environment and of particle collection capability. The following sections describe the experimental setup of the VMK at DLR-Cologne and the results of the tests.

5.1. Experimental Setup

The vertical test section facility is a blow down type wind tunnel with an open test section, capable of generating either subsonic or supersonic conditions in a vertical free stream. Measurement systems can be set up directly in the test chamber. Details of the conception and validation of the operating method can be found in [34]. Main facility components of the cold flow test apparatus are highlighted in Fig. 10a. In addition to high speed Schlieren visualization devices operating during all the cold flow tests, in-house seeding generator for dispersing solid particles is implemented. Inside the generator container, the particles are placed on a funnel-like shaker from where they
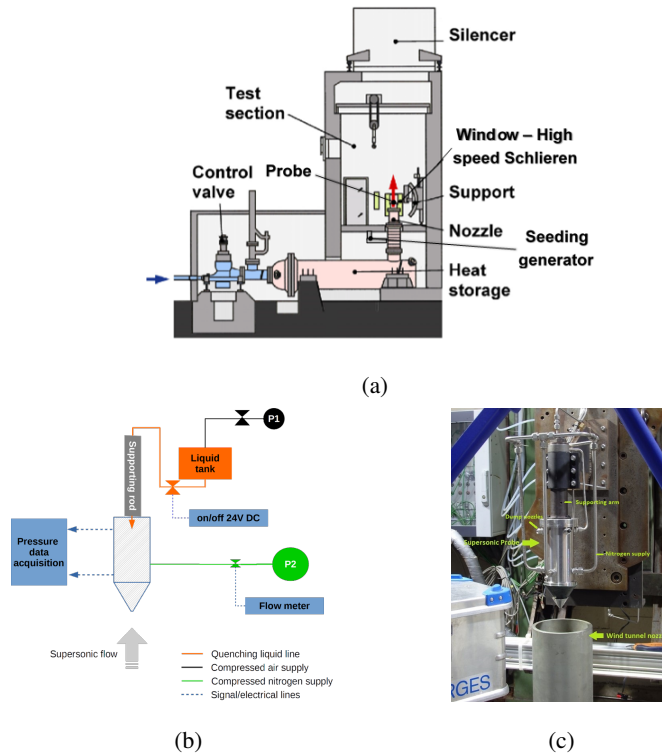
Figure 10: POLIMI-DLR Interface: (a) EMAP-VMK facility components (b) scheme of the probe implementation at the VMK; (c) details of facility.

trickle down in a fine line. Before reaching the floor, a percentage of the particle is inhaled by a suction pipe due to an applied overpressure.

The interface between the SPLab Probe and the VMK is shown in Fig. 10b. The quenching liquid tank is connected with a flexible hose to a compressed air vessel allowing a pressure inside the tank up to 12 *bar*. The tank connects to the probe by means of a pipe line featuring an electrovalve that controls the liquid provided to the injector. The quenching liquid pipe line is protected by the environment since it is inserted into the hollow supporting arm. Water has been used for the present test instead of C_2Cl_4. A relay switch circuit controlled by Arduino dictates the electrovalve opening and the closure, assuring the functioning of the injector for 1 s. A nitrogen tank supplies the secondary flow, whose mass flow rate is controlled by a Bronkhorst

25

Table 6: Cold Flow Tests conditions at different channel total pressure.

Exit Mach number M_e, [-]		3	
Area ratio ϵ, [-]		4.23	
Exit Static temperature T_{stat_e}, [K]		107	
Exit Velocity v_e, [m/s]		622.45	
VMK channel total pressure P_{tot_e}, [bar]	15	20	25
VMK channel mass flow rate $\dot{m}_{in}$, [kg/s]	0.0026	0.0035	0.0043
Nitrogen mass flow rate $\dot{m}_{N_2}$, [kg/s]		42	
Mass Ratio MR MR	16.1	12.1	9.7
Collected quenching liquid m_{quench}, [g]		59.7	

flowmeter (Bronkhorst IN-Flow F-116BI-IIU-90-V). The probe is connected to a supporting arm which is capable of motion in three directions by translation. It is set at a distance L=10 cm from the VMK exit section, centered with respect to the nozzle. Nitrogen flow employs three access points in the feeding line chamber, while the fourth access point is devoted to pressure transducer. Similarly, inside the collection chamber, one holes was devoted to the pressure measurement and the remaining three to the dump nozzles. This configuration makes the injection of nitrogen not symmetric and not equally distributed between N_2 injection points, thus giving rise to a spinning flow inside the probe that should enhance the mixing with the ingested mass flow rate. An ad-hoc tip was manufactured since the actual cold flow tests conditions require a smaller inlet diameter for granting the nominal mass flow ratio between the nitrogen and the ingested mass flow rate.

5.2. Experimental Results

Relevant properties of the cold flow tests are listed in Table 6. Tests represent off-design analysis proof of concept:

- test at 15 *bar*: check on fluid dynamic instabilities, due to supersonic-to-subsonic transition expected in the mixing chamber;

- test at 20 *bar*: supersonic mixing chamber, supersonic to subsonic transition expected at the head-end of the divergent;

- test at 25 *bar*: close to nominal conditions. Supersonic mixing chamber, supersonic to subsonic transition expected in the divergent;
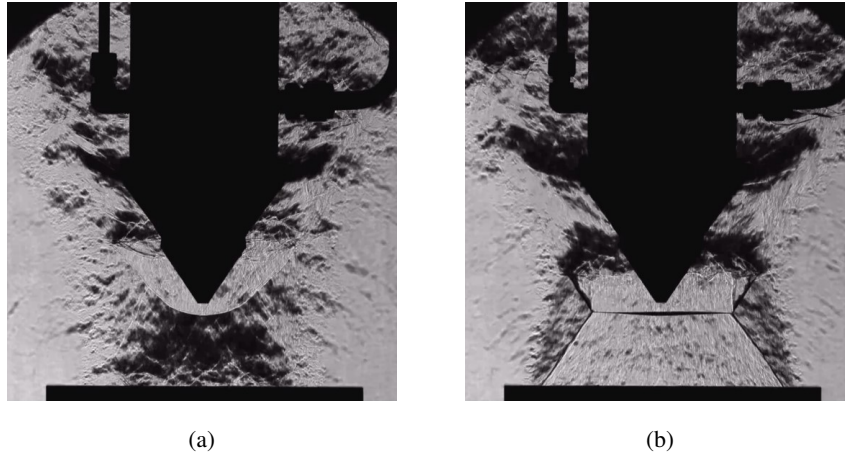

(a)   (b)

Figure 11: Schlieren images of the VMK tests. Moments of the starting transient: (a) initial bow shock; (b) bow shock disappearance. Test at total pressure of 15 bar.

Schlieren visualizations enabled the demonstration of the probe behaviour concept in relevant environment. The starting transient of the channel can be appreciated in Fig. 11. In particular, the generation of the inlet bow shock, a region featured by an intense density gradient, appears in front of the probe inlet and readily disappears. It is a typical behavior of a slightly supersonic flow, before reaching the nominal Mach number. At steady state conditions, the images show an attached oblique shock wave at the tip and a Mach disk at more advanced location with respect to the inlet plane: refer to Fig. 12. Both the conditions suggest the correct start-up of the probe and the absence of fluid dynamics instabilities due to off-design functioning causing the "unstart" of the probe and a bow-shock appearence in front of the device. Moreover, an actual supersonic flow inside the probe duct is demonstrated, since when momentum and energy of the flow cannot remain conserved in an inviscid flow across an oblique shock as it approaches the plume axis, a normal shock wave called Mach disc is formed, downstream of which the flow is subsonic. For an extensive dissusion of the plume phenomenology, refer to Simmons et al. [35]. Pressures in steady state conditions
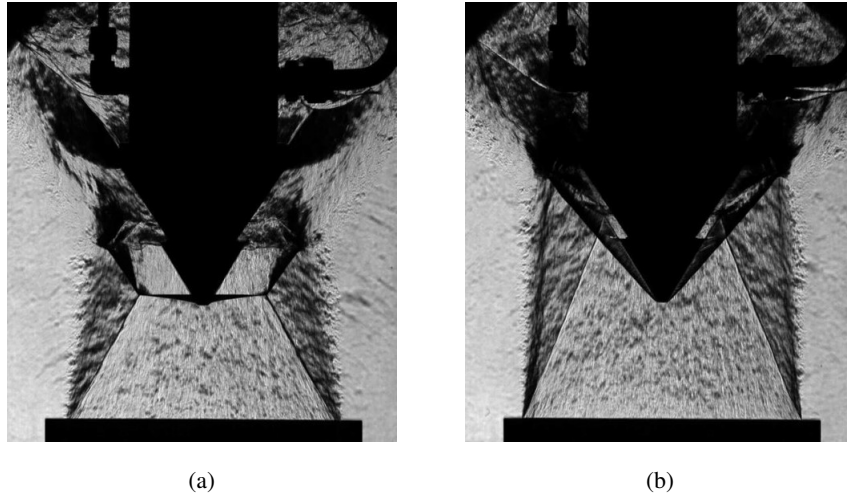
27

Figure 12: Schlieren images of the VMK tests at total pressure of (a) 15 bar; (b) 25 bar.

for the 25 *bar* test case for the nitrogen coolant flow and the collection chamber are 2.19±0.0035 *bar* and 1.84±0.0027 respectively. The results are in accordance with the nominal design prediction since the collection chamber pressure is expected to be lower than the nominal one (set at 2 *bar*, refer to Sec. 3.3.1), having a lower mass ratio and hence higher expansion in the divergent duct. The value of the nitrogen pressure in the stagnation chamber is in accordance with the one found in the CFD simulations.

Table 7: Particle size: comparison between collected MgO particles at different channel total pressure and the original particles.

	P, [bar]	d(0,1)	d(0,5)	d(0,9)	d(3,2)	d(4,3)
Original	-	7.15	14.6	26.2	5.693	17.032
	25	2.43	13.56	36.28	5.579	16.993

The collection technique was tested featuring the same experimental setup and implementing a seeding generator to seed the air with micrometric magnesium oxide particles. Qualitative results as a proof of concept of the collection technique are highlighted in Figure **??**.

The test were conducted at 25 *bar*, since it was the closest condition to the nominal design. The size distribution of the magnesium oxide collected was verified to check the
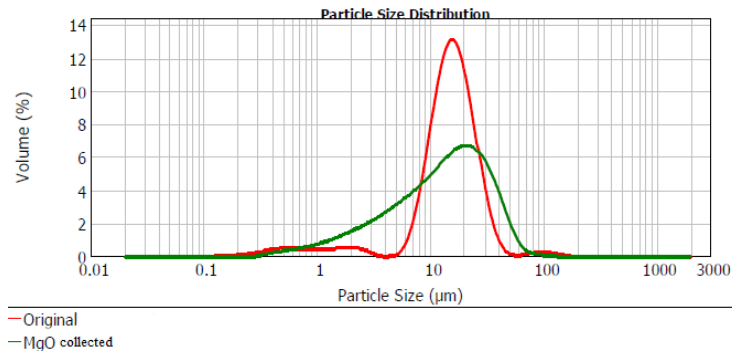
Figure 13: Particle size distribution: comparison between collected MgO particles at 25 *bar* and the original particles.

absence of important fragmentation or coalescence phenomena. The particle size distribution was obtained using laser diffraction methodology with Malvern Mastersizer 2000 instrument with water dispersion. The calculated values of the mean diameters (d10, d50, d90, d32, and d43) are listed in Table 7 and the volume based particle distribution is proposed in Fig. 13. It is interesting to see the absence of a substantial difference in terms of particle size distribution between the collected particles and the original magnesium oxide. Two possible minor effet could be underlined:

- possible particles fragmentation could have been arised due to water dispersion, since the magnesium oxide could have reacted with the liquid turning into magnesium hydroxide. The reader should be aware that the size distribution analysis was conducted one week after the cold flow collection tests. During the hot flow activtiy, particles will be analyzed immediately after the collection, minimizing possible chemical alteration;

- particles over 50 μ appear in Fig. 13. It must be noted that the obscuration computed by the Malvern Mastersizer was of 5.3, highlighting an important amount of material collected, that could have been subject to aggregation during the week before the analysis.

However, results in terms of d(4,3) and d(3,2) greatly fit the original size distribution mean diameter, suggesting an overall equality between the two batches of particles.

6. Conclusion

An innovative intrusive technique for the collection of the CCPs in the proximity of the rocket nozzle has been presented. The small device is put in the proximity of the nozzle to capture condensed particles before they react with the atmosphere and undergoing modifications due to velocity gradients or shock wave. The system design is very compact to limit incoming heat flux and influences on the external flow field.

The probe nose has a conical shape. This leads to the formation of attached oblique shock waves, allowing the rocket plume to enter the inlet duct while it is still supersonic. The flow is diluted with a cold supersonic inert gas. The resulting flow mixture is close to critical conditions and relatively cold. The gas enters a divergent nozzle where it crosses a normal shock wave, set by means of a back pressure. The flow keeps decelerating before entering the collection chamber, where a quenching liquid spray collects the condensed combustion products from the cold subsonic flow. The chamber is provided with exhaust nozzles in such a way that the combination of inlet gas and outflow guarantees the back-pressure necessary to generate the shock wave in the divergent.

The feasibility study has been conducted throught POLIRocket-V2, a quasi-1D code based on a mathematical approach proposed by Shapiro and a comparison with an axial-symmetric CFD calculations has been presented. A complex test case where an internal supersonic flow mixes with a cooling flow was considered. The comparison of Mach numbers, static pressure and static temperature was reported for the different flow regimes contained in the flow domain, including channel with friction, flow mixing, and overexpansion. A section-averaged comparison appears to be meaningful when using the axial-symmetric CFD data. With respect to the CFD approach, the quasi-1D method is less detailed and is not capable of capturing fluid dynamic effects that develop transversally with respect to the flow direction. The variable trends are correctly captured. The absolute numbers of the variables are not the same but the trends are shifted one respect to the other. The variations of the flow properties are similar in both of the cases. Most of the problems arise in all the processes that are intrinsically multidimensional. Oblique weak shock waves are not identified, being an

30

intrinsically more-than-1D process. As a consequence, pressure and temperature trends are smoother because shock trains are not captured. On the contrary, the location of normal shocks is properly captured. In the quasi-1D approach the mixing between two fluids seems to have a different duration between the two approaches. The reader should be aware that the flow mixing in the Shapiro approach requires a proper tuning for the length of the process and there is not a closed solution. In the presented case, it is clear that the stirring of the flow properties occurs faster than expected and a proper iterative work is requested on the POLIMI-V2 solver. In general, the approach proposed by Shapiro has a very low computational demand and demonstrates to be directly applicable in simple geometry cases. When more-than-1D processes develop within the flow, the code shows some limitations. Variable trends and variations are properly obtained. An activity for the tuning of different flow regimes and conditions with complete CFD solutions is progressing: miscible flow mixing, boundary layer growth, supersonic vs. subsonic cases represent some of the test cases that will be investigated in the near future.

Tests performed at DLR have preliminarily demonstrated the working principle of the collection technique. Supersonic cold flow tests at a representative Mach number and Schlieren visualization enabled to infer the transient and the steady state conditions. In particular, the bow shock in front of the inlet during the start up phase and the attached shock wave during the nominal functioning were appreciated. Collection of particles was demonstrated to occurr with the methodology proposed. Scheduled hot flow tests will enable the validation of the intrusive device investigated. A post-collection analysis with a laser diffraction methodology has been proposed. The size distribution, in particular the d(4,3) and d(3,2) of the collected particles, highlighted the substantial abscence of break up and coalescence phenomena inside the probe.

Acknowledgments

References

[1] D. Reydellet, Performance of rocket motors with metallized propellants.

[2] W. H. Miller, Solid rocket motor performance analysis and prediction, Vol. 8039, National Aeronautics and Space Administration, 1971.

[3] H. Carpenter, S. Morizumi, Thermal radiation from the exhaust plume of an aluminized composite propellant rocket, Journal of Spacecraft and Rockets 1 (5) (1964) 501–507.

[4] C. Voigt, U. Schumann, K. Graf, K.-D. Gottschaldt, Impact of rocket exhaust plumes on atmospheric composition and climate–an overview, EUCASS Proceedings Series–Advances in AeroSpace Sciences 4 (2013) 657–670.

[5] R. Sullivan, T. Thornberry, J. Abbatt, Ozone decomposition kinetics on alumina: effects of ozone partial pressure, relative humidity and repeated oxidation cycles, Atmospheric Chemistry and Physics 4 (5) (2004) 1301–1310.

[6] R. Bianco, J. T. Hynes, Heterogeneous reactions important in atmospheric ozone depletion: A theoretical perspective, Accounts of chemical research 39 (2) (2006) 159–165.

[7] M. Brennan, Recent combustion bomb testing of srm propellant, in: 32nd Joint Propulsion Conference and Exhibit, 1996, p. 3270.

[8] S. Gossé, L. Hespel, P. Gossart, A. Delfour, Morphological characterization and particle sizing of alumina particles in solid rocket motor, Journal of propulsion and power 22 (1) (2006) 127–135.

[9] O. Glotov, D. Yagodnikov, VorobEv, V. Zarko, V. Simonenko, Ignition, combustion, and agglomeration of encapsulated aluminum particles in a composite solid propellant. ii. experimental studies of agglomeration., Combustion, Explosion, & Shock Waves 43 (3).

[10] J. Hijlkema, P. Prévot, M. Prévost, V. Mironov, Particle size distribution measurements in the keldysh research centre experimental setup at onera, in: 47th AIAA/ASME/SAE/ASEE Joint Propulsion Conference & Exhibit, 2011, p. 5712.

[11] S. Gallier, J.-G. Kratz, N. Quaglia, G. Fouin, Detailed analysis of a quench bomb for the study of aluminum agglomeration in solid propellants, Progress in Propulsion Physics 8 (2016) 197–212.

[12] F. Maggi, S. Dossi, L. T. DeLuca, Combustion of metal agglomerates in a solid rocket core flow, Acta Astronautica 92 (2) (2013) 163–171.

[13] L. H. Caveny, A. Gany, Breakup of al/al2o3 agglomerates in accelerating flowfields, AIAA Journal 17 (12) (1979) 1368–1371.

[14] F. E. Marble, Droplet agglomeration in rocket nozzles caused by particle slip and collision, Astronautica Acta 13 (2) (1967) 159–166.

[15] C. T. Crowe, P. G. Willoughby, A study of particle growth in a rocket nozzle., AIAA Journal 5 (7) (1967) 1300–1304.

[16] H. Cheung, N. S. CoHEN, Performance of solid propellants containing metal additives, AIAA Journal 3 (2) (1965) 250–257.

[17] B. Brown, K. P. McArty, Particle size of condensed oxides from combustion of metalized solid propellants, in: Symposium (International) on Combustion, Vol. 8, Elsevier, 1961, pp. 814–823.

[18] P. A. Kessel, Rocket exhaust probe, uS Patent 4,662,216 (1987).

[19] M. Danilin, P. Popp, R. Herman, M. K. Ko, M. Ross, C. Kolb, D. Fahey, L. Avallone, D. Toohey, B. Ridley, et al., Quantifying uptake of hno3 and h2o by alumina particles in athena-2 rocket plume, Journal of Geophysical Research: Atmospheres 108 (D4).

[20] R. Sehgal, An experimental investigation of a gas-particle system, Tech. rep., DTIC Document (1962).

[21] R. A. Dobbins, L. D. Strand, A comparison of two methods of measuring particle size of al2o3 produced by a small rocket motor, AIAA Journal 8 (9) (1970) 1544–1550.

[22] R. H. Carns, G. Armstrong, R. H. Rast, D. R. Mitchell, Rocket motor exhaust scrubber, uS Patent 6,964,699 (2005).

[23] A. H. Shapiro, The dynamics and thermodynamics of compressible fluid flow, John Wiley & Sons, 1953.

[24] V. Babuk, V. Vasilyev, M. Malakhov, Condensed combustion products at the burning surface of aluminized solid propellant, Journal of Propulsion and Power 15 (6) (1999) 783–793.

[25] T. Fedotova, O. Glotov, V. Zarko, Chemical analysis of aluminum as a propellant ingredient and determination of aluminum and aluminum nitride in condensed combustion products, Propellants, Explosives, Pyrotechnics 25 (6) (2000) 325–332.

[26] O. Glotov, Condensed combustion products of aluminized propellants. iii. effect of an inert gaseous combustion environment, Combustion, Explosion and Shock Waves 38 (1) (2002) 92–100.

[27] O. Glotov, V. Y. Zyryanov, Condensed combustion products of aluminized propellants. 1. a technique for investigating the evolution of disperse-phase particles, Combustion, Explosion, and Shock Waves 31 (1) (1995) 72–78.

[28] D. Viganò, A. Annovazzi, F. Maggi, Monte carlo uncertainty quantification using quasi-1d srm ballistic model, International Journal of Aerospace Engineering 2016.

[29] W. H. Press, Numerical recipes 3rd edition: The art of scientific computing, Cambridge university press, 2007.

[30] Anon, Homepage of dlr tau code, last Visit: 13/01/2018.
URL http://tau.dlr.de/code-description/

34

[31] R. B. Bird, Transport phenomena, Applied Mechanics Reviews 55 (1) (2002) R1–R4.

[32] J. D. Anderson, Modern compressible flow: with historical perspective, Vol. 12, McGraw-Hill New York, 1990.

[33] K. Matsuo, Shock train and pseudo-shock phenomena in supersonic internal flows, Journal of Thermal Science 12 (3) (2003) 204–208.

[34] Vertical test section cologne (vmk), supersonic and hypersonic technology department.
URL `http://www.dlr.de/as/en/desktopdefault.aspx/tabid-194/407_read-5445/`

[35] F. S. Simmons, Rocket exhaust plume phenomenology, Aerospace Corporation, 2000.